CANADIAN JOURNAL OF EXPLORATION GEOPHYSICS
VOL. 33, NOS.1 & 2 (DECEMBER 1997), P. 8-20

ADVANTAGES OF PARABOLIC REPRESENTATION OF CURVED INTERFACES IN 2D RAY SEISMOGRAM COMPUTATION

F. HRON[1]

ABSTRACT

In seismic numerical modeling, curved interfaces of two dimensional models are frequently represented by cubic splines which are applied to the sets of discrete points specifying individual boundaries. Unfortunately, when the cubic splines are applied to even modestly scattered input points, conspicuous unjustified overshooting and unrealistically high undulating shape are observed on the lines representing the interfaces. These obvious artifacts lead to computational difficulties in the production of synthetic seismograms based on the ray approach, since the wavy shape of interfaces, combined with high crests and deep troughs produced by the overshooting, increases the number of multiple arrivals of the same type of rays, most of them with very small amplitudes. We demonstrate that both the overshooting, and the undulating shape of the cubic spline representations, are caused by two intrinsic properties of the cubic spline, namely by its continuity up to the second order, and by the fact that the spline has to pass through each point of the set which it approximates. Hence the cubic spline representation of the seismic boundaries is inconvenient for the computation of ray based synthetic seismograms and should be replaced by an alternative technique. We found such a method in the so-called parabolic approximation, which was originally proposed by Marcinovskaya and Krasavin. It is based on second order polynomials which are allowed to miss some of the input points within a prescribed tolerance, thereby significantly reducing the undulating shape of the mathematical representation of the interface. The undesirable overshooting is completely eliminated with the help of the so-called inserted parabolas. A brief description of the method, together with the basic formulae, is presented in the Appendix. Practical applications of the method are demonstrated on numerical examples which also provide supporting evidence for the physical justification of the method and discussion of its features.

INTRODUCTION

Most of the methods used nowadays for the interpretation of seismic data or their imaging are based on the ray concept. This explains an ongoing interest in the ray methods and a considerable effort spent on the improvement of their efficiency and greater accuracy by many researchers both in the oil industry and research institutions. As a result, a steadily increasing number of software applications, which are being developed for the needs of the oil industry, employs the concept of rays.

Regardless of the specific nature of individual ray approaches, each ray theory is based on a basic assumption that the total wave field can be decomposed into individual contributions, each of them associated with a particular ray path, along which the seismic energy travels from the source to the receiver. Hence during the computation of ray based seismograms one of the major tasks is the construction of the so-called partial ray expansion, which is the selection of the finite number of rays whose contribution to the total seismic field is to be evaluated. Needless to say that the quality of the ray based synthetic seismograms, i.e., their resemblance with the total seismic field, is directly influenced by the set of rays assembled into the partial ray expansion. Consequently, one can obtain even for the same model and using the same computer program quite differently looking synthetic seismograms, if different sets of rays had been used during the computation (Hron et al., 1974). Quite naturally, a computer based ray generation scheme (Hron 1971, 1972 and 1973) should be used when all significant arrivals are to be captured on synthetic traces.

During the actual computation of synthetic seismograms most of the CPU time is inevitably spent on two point ray tracing which is needed to secure that each ray arrives at a specified receiver location. In principle, the two point ray tracing procedure is relatively simple for homogeneous layers separated by plane interfaces when the travel time

$$\tau = \tau\,(x\,(\theta_o)) \tag{1}$$

and the offset

$$x = x\,(\theta_o) \tag{2}$$

are monotonous functions of the taking-off angle θ_o at the source.

The two point ray tracing becomes more complicated when the monotonous property of the functional dependence (2) of the offset on the taking-off angle θ_o disappears and the multiple arrivals of the same type of rays, like the first unconverted P primaries in Figure 1a, occur at some receivers. Such a situation is clearly manifested by the

Manuscript received by the Editor...

[1]Department of Physics, University of Alberta, Edmonton, Alberta, Canada T6G 2J1

This research has been supported in part by NSERC Operating Grant 9157 and by the NATO Linkage Grant. ENVIR.LG940714. Numerical examples presented in the paper were produced by Hu-shun Zhou. Appreciation is also expressed to two anonymous reviewers whose constructive suggestions resulted in the improvements of the original discussion of the numerical results.

appearance of several simple branches on the travel time curve (see 29 simple branches in Figure 2a, with the image of some of them shrunk almost to a point because of the scale chosen). Each of these simple branches corresponds to the non-overlapping intervals of the taking-off angle θ_o, in which the monotonous properties of (1) and (2) are preserved, thereby permitting once again a straightforward, albeit numerically quite demanding, two point ray tracing within each individual simple travel time branch. Only then, after numerically determining on each travel time branch the appropriate taking-off angle θ_o, at which the ray has to be radiated from the source to reach the receiver at a given offset x, the travel time and amplitude of the ray can be computed and its contribution to the synthetic seismogram evaluated. It is at this stage, when quite a few of the truly existing ray paths are eliminated from the computation, after it is found that their ray amplitudes fall below a predefined threshold thereby indicating their insignificant contribution to the ground motion registered by the receiver.

This process of elimination of the "weak" ray contributions, which should be carried out automatically by any efficient computer code, is worth demonstrating on the synthetic data due to its direct bearing on the main topic of this paper. We will do it by examining the amplitude-distance curves of the first unconverted P primaries displayed in Figure 3a and corresponding to the set of 29 separate branches shown in Figure 2a. We can see in Figure 2a that although 4 different arrivals, each of them travelling along a different ray path from the surface source located at x_s = 36 km to the receiver at x = 42 km, exist, it is the earliest one (with the travel time of t_1 = 7.57s) which will play the dominant role due to its relative amplitude of A_1 = 0.002 being almost four times stronger (see Fig. 3a) than those of the remaining three events, whose travel times are, according to Figure 2a, t_2 = 9.00s, t_3 = 10.78s and t_4 = 14.41s, respectively. Please note that the simple travel time branch and the amplitude-distance curve pertinent to the strongest primary are labelled by "*" in Figures 2a and 3a for easy identification.

Thus for many practical purposes and especially in the early stages of numerical modelling, when we are usually interested in the main features seen on the seismic records, it might be quite sufficient if only the strongest arrivals are retained in the computation, while those with smaller amplitudes are discarded thereby eliminating all the pertinent computer effort which would otherwise be needed for their computation. It is easily understood that any method that would eliminate in the early stages of computation the rays with insignificant amplitudes would considerably improve the computational efficiency of the program.

In practice, such a goal can indeed be achieved, for example, by a suitable mathematical representation of input data characterizing a given geological model. The results of such a procedure are shown in Figure 2b, in which we can find for a receiver located at the offset x = 42 km only one arrival with the travel time and amplitude almost identical to those ascribed in Figures 2a and 3a to the strongest arrival labelled by "*". This equivalent ray travels through the same geological structure characterized by the same input data that were represented this time, however, by a new version of the geological model, in which we used parabolic representations rather than cubic splines for the mathematical approximation of interfaces (compare Figures 4a and 4b, where both versions of interfaces and the corresponding bundles of rays are shown). In this case the reduction in number of simple travel time branches of the first unconverted primaries (down from 29 in Fig. 2a, to 18 in Fig. 2b) was simply accomplished by employing a new parabolic approximation procedure for interfaces, which is described in the Appendix.

Both structures shown in Figure 1 are two different versions of the same simplified two layered crust proposed for Southern Alberta by Kanasewich (1968). Its elastic parameters are given in Table 1 and the points characterizing the boundaries in this 2D structure are marked by crosses in Figure 5. It should be mentioned that we have chosen Kanasewich's model for the computation of the illustrative numerical examples because of the absence of the velocity gradients in his version of the crust. In this way we could easily demonstrate numerically a rather strong dependence of the multiplicity of travel time branches on the undulating shape of seismic boundaries and propose the means for suppressing this undesirable artifact.

A similar, and well known influence of the velocity gradients on the multiplicity of travel time branches was recently investigated by Zhou (1996). He showed that although the strong velocity gradients do increase the number of simple travel time branches, the main complications caused by the gradients are to be seen in the formation of "cusps" on the travel time branches seen in Figure 2. They are clear indicators of caustics (focal lines) in the vicinity of which the standard version of the Asymptotic Ray Theory cannot be used for the ray amplitude computation and an alternative high frequency approach, similar to that developed by Choi and Hron (1981), must be employed.

Having in mind the scope of this paper and its tutorial character, most of our reasoning and demonstrations of advantages for using parabolic approximation of seismic interfaces for a convenient and physically justified reduction of travel time branches will be based on the numerical examples. These were obtained with the help of computer software described in detail by Zhou (1996). The pertinent computer code is based on the Asymptotic Ray Theory (Babich and Alekseev, 1958; Hron, 1968; Hron and Kanasewich, 1971; Cerveny and Ravindra, 1971) and its extensions Cerveny and Hron, 1980; and Choi and Hron, 1981). The main features of this ray theory are well described in these references. Its application to the computation of synthetic seismograms for layered structures with various degrees of inhomogeneity and anisotropy was shown by Hron et al. (1977) or Hron et al. (1986), among others.

Formulation of the Problem and its Solution

In two dimensional models seismic boundaries are represented by continuous lines z = z(x) in a vertical, say (x, z)

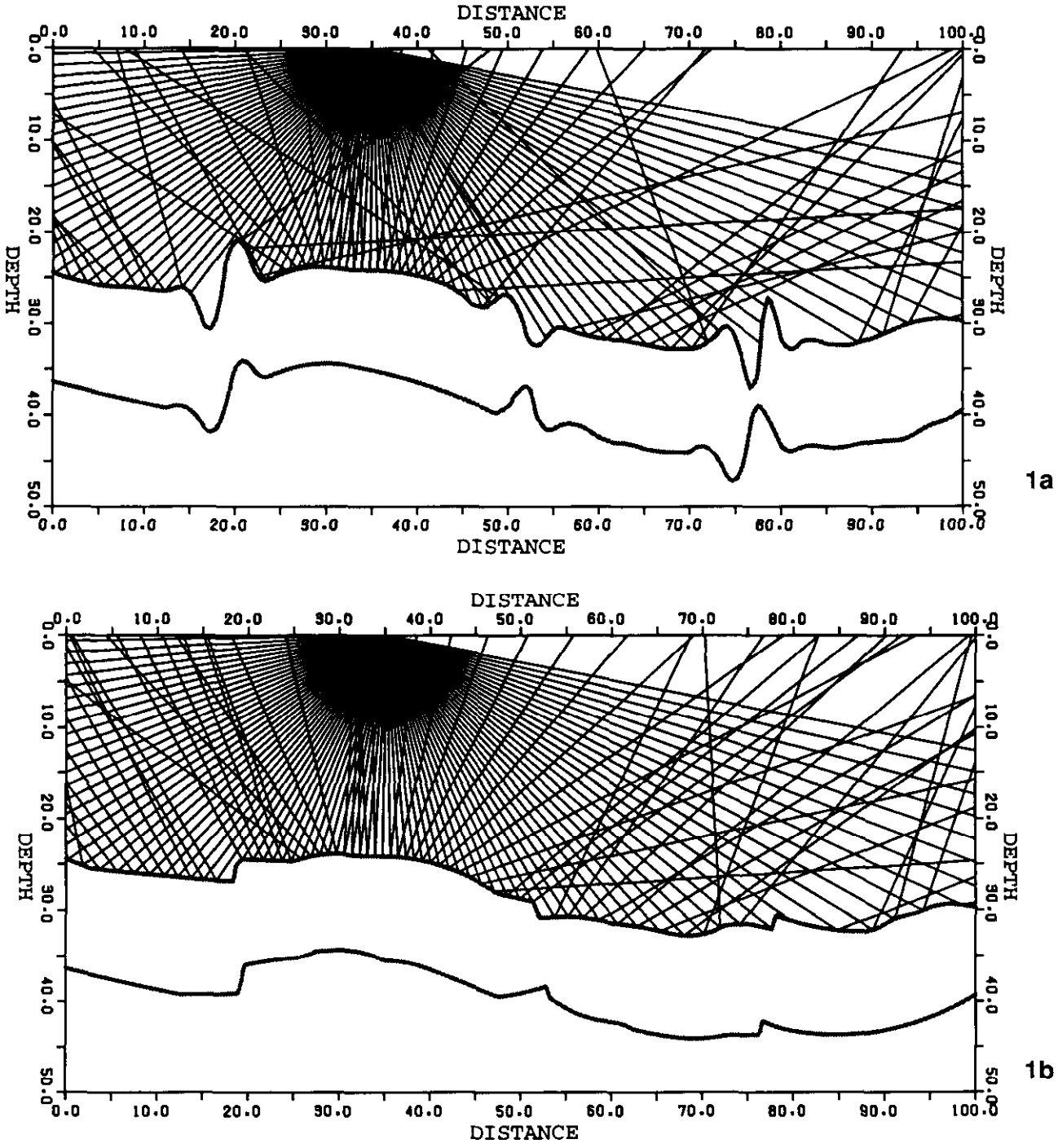

Fig. 1. Ray paths of the first unconverted *P* primaries computed for two versions of a simplified two-dimensional crust given in Table 1. Both versions differ only in the mathematical representations of two inner interfaces specified by the same set of discrete points marked by crosses in Figures 5a and 5b, where only the interfaces are displayed. Interfaces in Fig. 1a were represented by the cubic splines. The pertinent travel times and amplitude distance curves are displayed in Figures 2a and 3a, respectively. In Fig. 1b the so-called parabolic approximation for both inner boundaries was employed. The corresponding travel times and amplitude distance curves are shown in Figures 2b and 3b, respectively.

plane. In a vast majority of oil exploration related problems, each of the curved seismic boundaries is characterized by a set of M discrete points specified in our Cartesian coordinate system (x, z) by their coordinates $[\xi_m, \zeta_m]$, m = 1, ..., M. This leaves each researcher with considerable freedom regarding the selection of a specific mathematical representation of the curve z = z(x) approximating the boundary. Very often the cubic splines are used for this purpose, as we did in Figures 1a and 5a.

Mathematically, the cubic spline for M discrete points $[\xi_m, \zeta_m]$, m = 1, ..., M, is defined as a cubic polynomial

$$z_m(x) = \alpha_m(x-\xi_m)^3 + \beta_m(x-\xi_m)^2 + \gamma_m(x-\xi_m) + \zeta_m,$$

$$\xi_m \le x \le \xi_{m+1}, 1 \le m \le M\text{-}1 \qquad (3)$$

with (M-1) triplets of coefficients α_m, β_m, γ_m determined from the required continuity up to the second derivative of the spline (3) over the entire range $\xi_1 \le x \le \xi_M$ of definition.

A detailed study of the continuity requirements at all (M-2) internal points $[\xi_m, \zeta_m]$ reveals (see for example, Ahlberg et al., 1967; or Forsythe et al., 1977) that once the one-sided second derivatives $\frac{d^2z}{dx^2}$ are specified at both endpoints of the set, each triplet of coefficients α_m, β_m and γ_m is evaluated in terms of Cartesian coordinates of only 3 adjacent points $[\xi_{m-1}, \zeta_{m-1}]$, $[\xi_m, \zeta_m]$ and $[\xi_{m+1}, \zeta_{m+1}]$, $1 < m < M$. This fact makes computation of the triplets of coefficients very efficient and explains why the cubic splines have become so popular for the interpolation and mathematical representation of the sets of discrete points in many branches of sciences.

Unfortunately, we have already presented evidence both in the form of physical reasoning and the numerical results (see Fig. 2a and 2b), showing that in spite of a rather widely spread usage by many seismologists, the cubic splines are not well suited for mathematical representation of seismic boundaries in 2D models, if any procedure based on the ray tracing is to be used.

A classical example of a rather limited suitability of cubic splines for the seismic boundary representation, when the ray tracing is involved, is given in Figure 1a. We showed in that figure cubic spline representations of seismic boundaries for a simplified version of a two layered model, which was proposed for Southern Alberta by Kanasewich (1968) (see Table 1 for details). In our example two curved interfaces, which represent bottoms of the first and the second homogeneous layers, were specified by two sets of discrete points. These input points are marked by crosses in the corresponding Figure 5a, in which only the seismic interfaces from Figure 1a are reproduced in order to facilitate discussion of their approximations. We see immediately in Figures 1a and 5a that the cubic spline representation of both curved boundaries produced unrealistic overshooting at all six segments of the boundaries with almost vertical slopes. Please note that several rays had to be truncated at these steep parts of the interface, since had they been continued after their reflection, they would have struck the same interface again. The second reflection from the same reflector would have made them ineligible to be classified as the first unconverted primaries.

Table 1. Elastic parameters for a homogeneous two-layered model of the Southern Alberta Crust.

	V_p (km/s)	V_s (km/s)	ρ(g/cm^3)
Layer 1	6.5	3.75	2.8
Layer 2	7.2	4.16	3.2
Half-space	8.2	4.73	3.45

The highly undesirable effects of these artifacts on any ray shooting procedure is easily understood since they will lead to the creation of false shadow regions, as is seen in Figure 1a, where the rays of the first unconverted P primaries radiated from a surface point source located at x_s = 36 km are displayed. Moreover, the sharp curvatures at the crests and troughs of each overshooting will scatter the rays almost over the entire model thereby creating false multiple arrivals and broken travel times curves as it is shown in Figure 2a. This also causes additional unwelcome numerical complications, since the exact positions of bounds of the interval $\langle\tilde{\theta}_1, \tilde{\theta}_2\rangle$ defining the range of the taking-off angles for each simple branch, must be determined before any two point ray tracing.

Obviously the existence of 29 simple travel time branches seen in Figure 2a cannot be explained by the overshooting alone. As it turns out, the multiplicity of simple branches on the travel time curves is also caused by the wavy shape of the spline function (3), in which the concave $\left(\frac{d^2z_m}{dx^2} > 0\right)$ and convex $\left(\frac{d^2z_m}{dx^2} < 0\right)$ parts of the curve, as seen by the observer on the surface, are smoothly linked together. This phenomenon is depicted in Figure 1a, where we can see that the concave segments of the interface, acting like a concave mirror, have a tendency to focus the reflected rays, whereas the convex parts of the boundary have a diverging effect on the reflected rays, similar to that which has a convex mirror on the light rays in geometrical optics. It is not difficult to see that both the overshooting, and the wavy character of the spline function (3) are unavoidable whenever the cubic spline is applied even to a modestly scattered set of points, since both phenomena are the direct consequence of two intrinsic properties of the cubic spline, namely its continuity and its passage through each input point, respectively. Both properties are easily deduced from the cubic spline definition (3) and verified in Figure 5a.

Thus we can conclude that the use of cubic splines for mathematical representation of curved seismic boundaries is, in principle, inconvenient as it leads to computational complications that are directly linked to two intrinsic properties of the cubic spline mentioned in the foregoing. It is also clear that any suitable replacement for the cubic spline will have to be devoid of the same properties meaning that such mathematical approximation should have a discontinuous second derivative and should be allowed to miss some input points within a tolerance specified in input.

In our opinion, we have found such a suitable alternative in the method which was originally developed by Marcinovskaya and Krasavin (1968), mathematical details of which are given in the Appendix. It is explained there that in accordance with (A1) the seismic boundary is now represented by a set of I parabolas which are smoothly linked together at the end points of the non-overlapping intervals $\langle X_i, X_{i+1}\rangle$, over which a second order polynomial

$$z_i(x) = a_i x^2 + b_i x + c_i,\ 1 \le i \le I, \qquad (4)$$

is employed for a parabolic approximation of the seismic

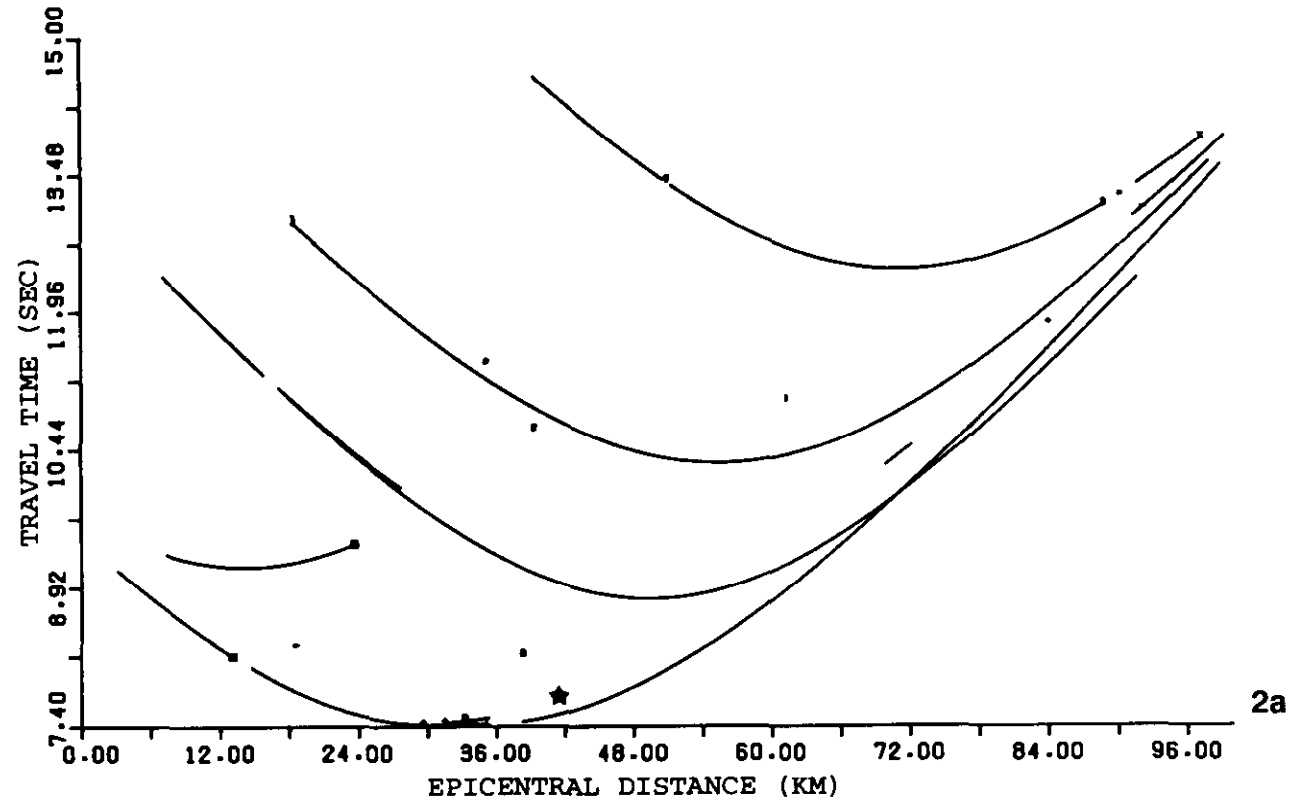

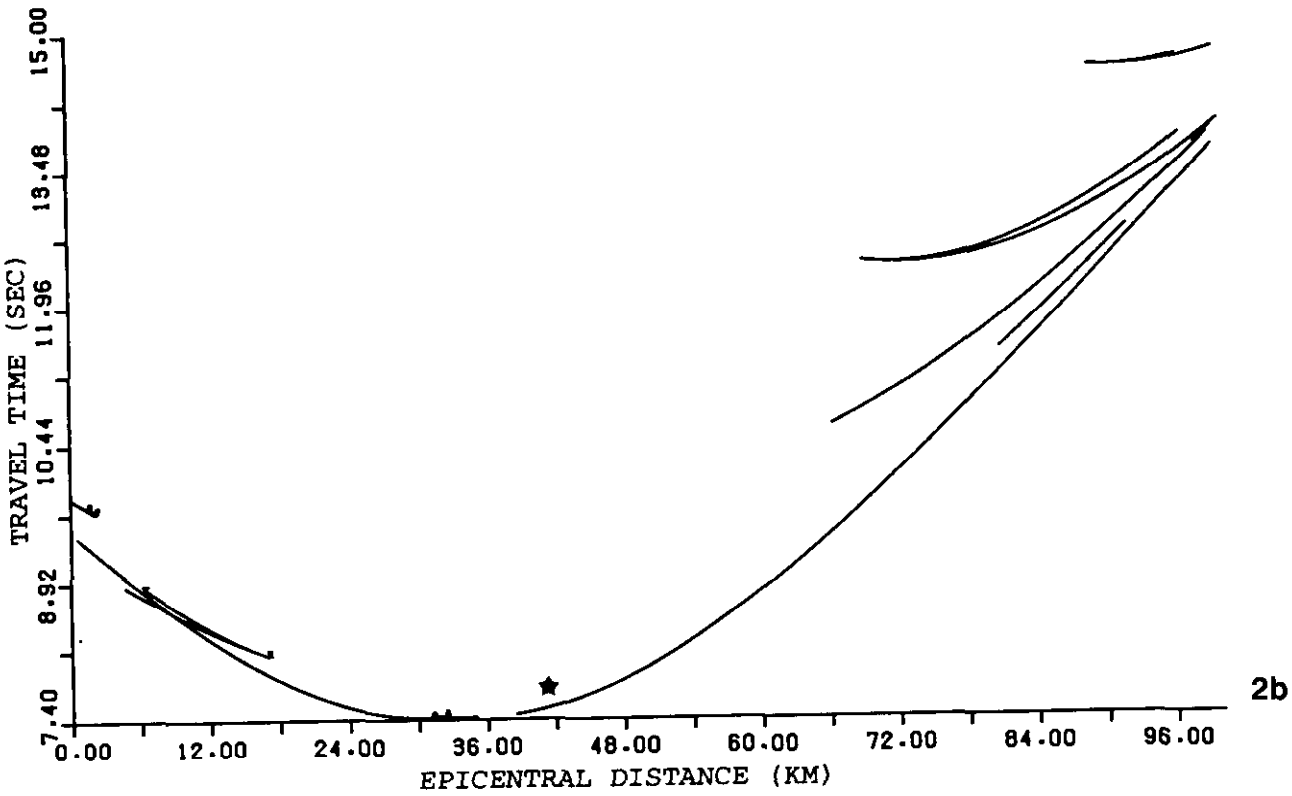

Fig. 2. Travel time curves of the first unconverted P primaries pertinent to the ray paths in Figure1. Note that some of the separate branches are contracted almost to a point because of the scale chosen for the epicentral distances (offsets). The travel time branches corresponding to the first arrivals at the range from 38 km to 100 km are marked in both versions by "*" for easy reference. There are 29 separate branches in Figure 2a corresponding to the ray paths in Figure 1a, and 18 branches in Figure 2b related to the ray paths in Figure 1b.

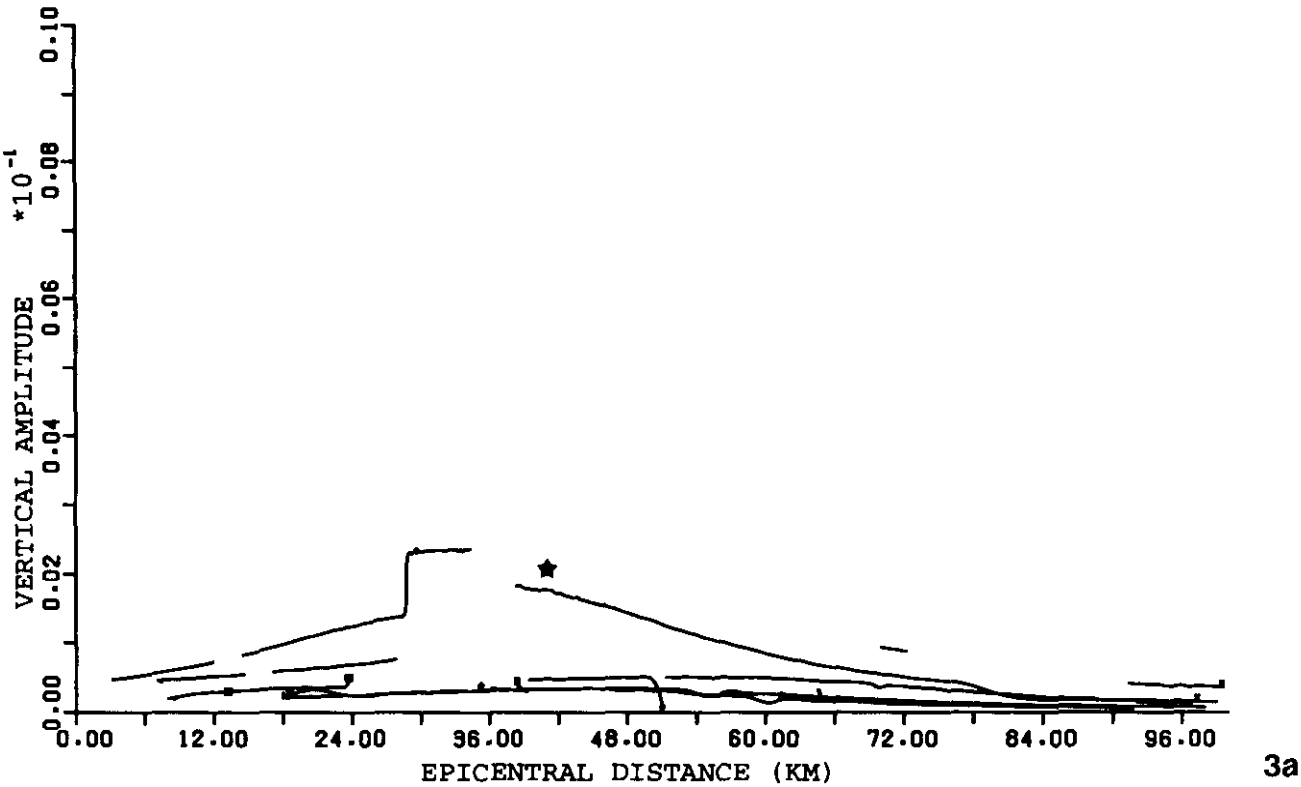

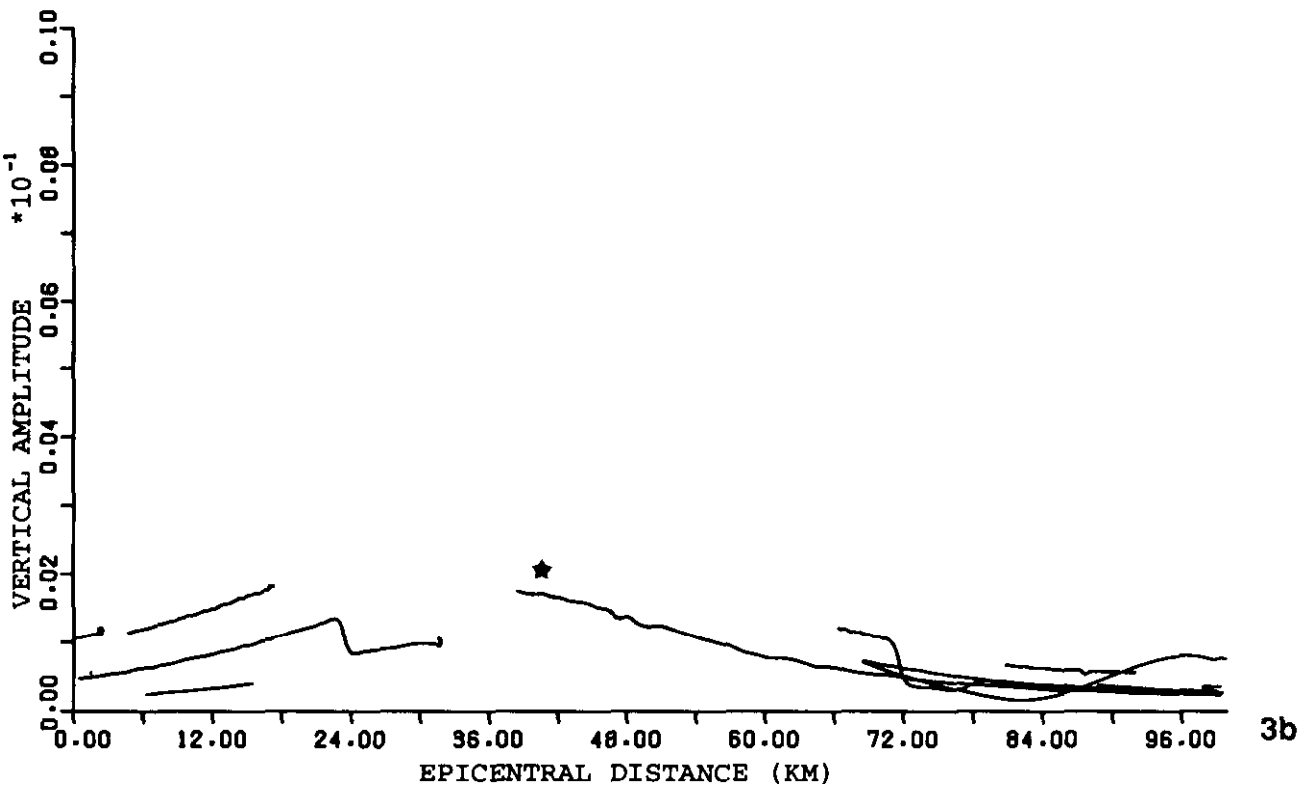

Fig. 3. Amplitude distance curves of the first unconverted P primaries with ray paths shown in Figure 1. The amplitude distance curves marked by "*" in each version correspond to the travel time branches of the first arrivals also marked by "*" in Figure 2. Note that only amplitude curves for extended (i.e., not contracted to a point) travel time branches in Figure 2 are easily recognizable. There are 13 amplitude distance curves in Figure 3a corresponding to 13 extended travel time branches in Figure 2a, and 12 of them in Figure 3b, which are related to 12 extended travel time branches in Figure 2b.

boundary. This time the local concave $\left\{\frac{d^2z}{dx^2}<0\right\}$ or convex $\left\{\frac{d^2z}{dx^2}>0\right\}$ shape of each polynomial (4) remains unchanged over the entire range $\langle X_i, X_{i+1}\rangle$ of the boundary segment which it approximates (as opposed to the cubic spline representation (3), where it can change). In this manner, the wavy character of the parabolic representation of the boundary specified by M input points $[\xi_m, \zeta_m]$, $1 \le m \le M$, is reduced. Furthermore, as the parabolic representation is not required to pass exactly through every input point, the number I of the individual parabolic segments is generally smaller than the number of cubic segments (M-1) on the spline, which has to go through each input point. In this way, the undulating shape of the

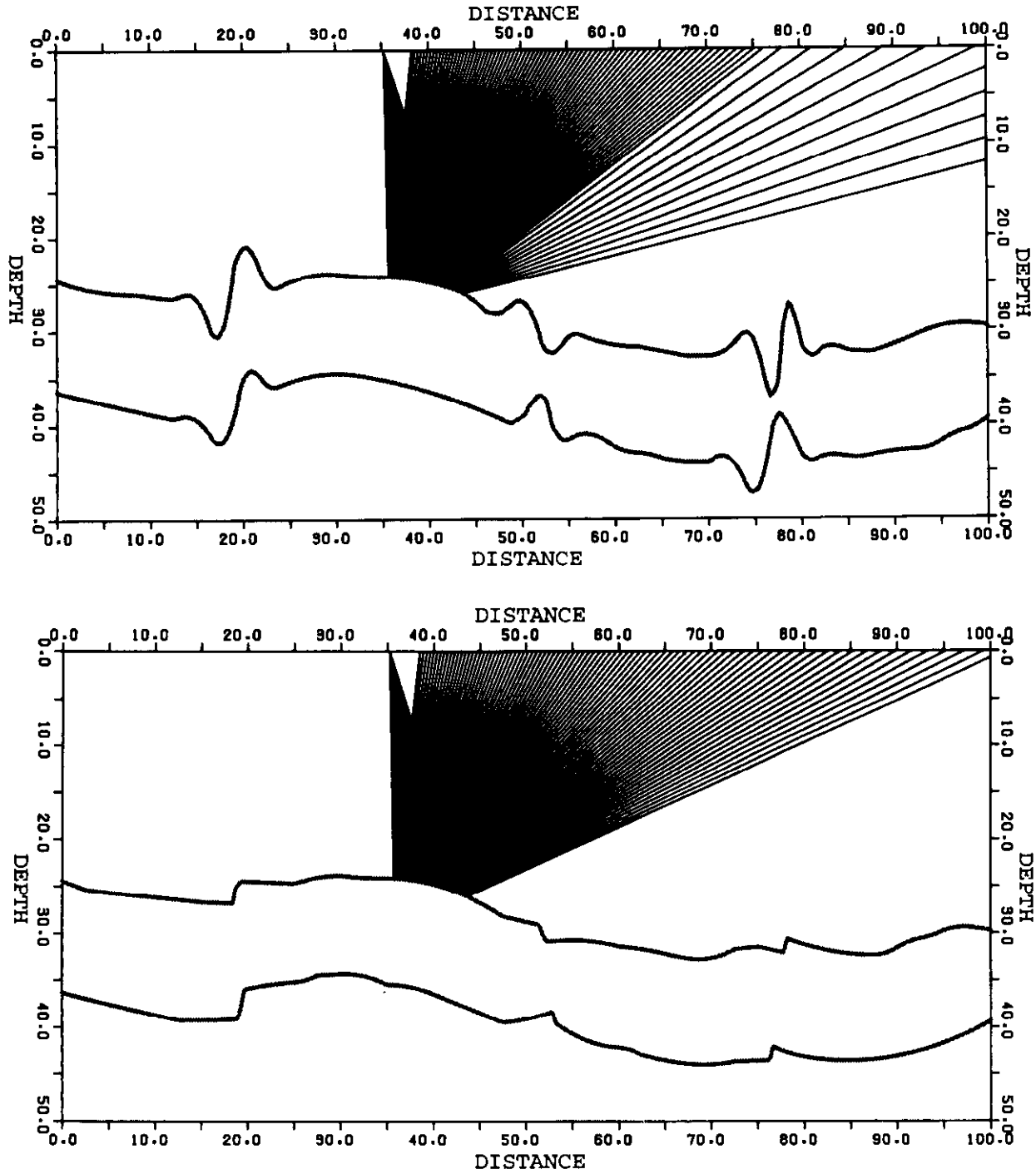

Fig. 4. Two corresponding bundles of rays pertinent to the first arrivals whose travel time branches are labelled by "*" in Figure 2. The rays in Figure 4a were obtained for the cubic spline approximation of interfaces in Figure 1a, whereas the rays in Figure 4b were computed for the parabolic representation of the boundaries in Figure 1b. Note that a variable step in taking-off angle was employed when drawing the rays in Figure 4a to demonstrate a flexibility of the ray shooting procedure.

parabolic representation is further suppressed (compare for example, the previously discussed Figure 5a with Figure 5c displaying parabolic representations of the seismic boundaries specified by the same sets of input points). As a result, the number of simple branches on the travel time curves of the first unconverted P primaries computed for the model in Figure 6 and displayed in Figure 7a dropped to 5, well down from the original number of 29 in Figure 2a.

It only remains to be added that by eliminating the overshooting in the parabolic representation of the steep segments of the boundaries, which was achieved with the help of inserted parabolas described in the Appendix, we further simplified the ray tracing procedure as its result displayed in Figure 6 testifies. It shows a highly regular pattern of rays, in which no false shadow zones and highly scattering parts of reflectors, all of them caused by spurious overshooting in Figure 1a, exist, thereby increasing the physical justification of the pertinent numerical results.

Discussion of Numerical Results

Although most of the numerical results presented in this paper have already been employed in the previous two sections as numerical evidence for our reasoning, a unified, final review of a few selected figures will be given next. It will allow us to formulate several practical conclusions concerning the use of different representations of the same set of input points specifying seismic interfaces in 2D ray tracing. In particular, we will demonstrate how we can influence, by a suitable choice of the relative error parameter ε (see Eqs. (A5) in the Appendix), the relative amplitude of events admitted to the synthetic seismogram computation, thereby controlling the amount of detail displayed on synthetic traces. For this purpose we will examine travel times and amplitudes of the first unconverted P primaries computed for two different versions of the parabolic approximation of the same set of input points specifying seismic boundaries in a simplified version of the Southern Alberta crust model proposed by Kanasewich (1968) and already used in our discussions in the previous two sections. The elastic parameters of the model are given in Table 1, whereas geometrical shapes of 3 different representations of the seismic interfaces of the model, all of them based on the same set of input points, are displayed in Figure 5.

This time we will start with Figures 5b and 5c in which the parabolic representations of the boundaries corresponding to $\varepsilon = 0.1$ and $\varepsilon = 0.4$, respectively, are displayed. As expected, by increasing the relative error ε, with which the parabolic representation (4) is allowed to miss some individual input points marked by crosses, the number I of different parabolic segments in each interface representation should decrease, thereby also decreasing the number of simple branches in the pertinent travel time curves, as we explained in the previous section. Our expectations are indeed supported by the evidence in Table 2, according to which the reduction in the number of individual parabolas, approximating the bottom of the first layer, from 44 (in Fig. 5b and also in Fig. 1b) to 21 (in Fig. 5c and Fig. 6), resulted in the decrease of the simple

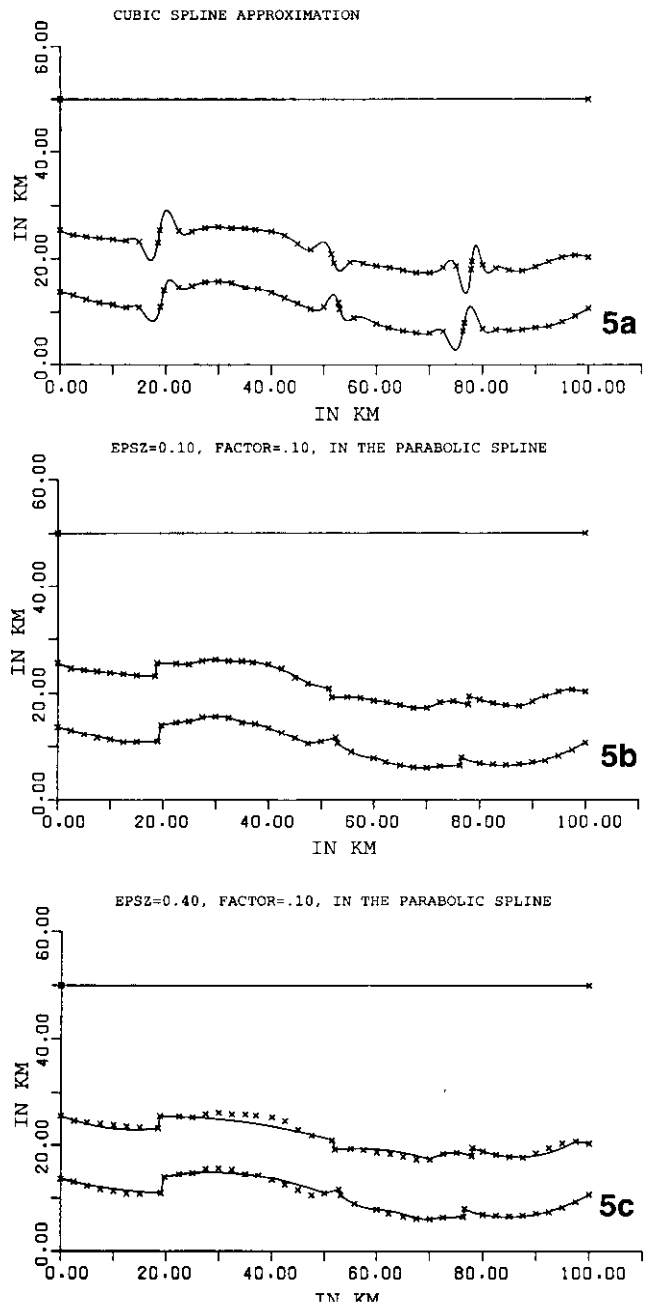

Fig. 5. Three different representations of the same sets of points specifying interfaces in a simplified two layered crust from Southern Alberta. The input points are marked by crosses and identical scales are used for all three versions of the model, in order to facilitate comparison. Note that the vertical axes are oriented this time positively upward with the zero reference point situated at the depth of 50 km below the surface. The positive upward orientation of the vertical axis is used in the usual application of our version of the parabolic approximation. The standard cubic spline approximations are shown in Figure 5a, whereas two different parabolic representations, each for different values of the tolerance parameter ε are displayed in Figure 5b ($\varepsilon = 0.1$) and Figure 5c ($\varepsilon = 0.4$), respectively. The mathematical definition of ε is given by Equation A5 in the Appendix.

travel time branches of the first unconverted P primaries from 18 (in Fig. 2b) to a mere 5 (in Fig. 7a).

At this point the question of consistency arises, as the dif-

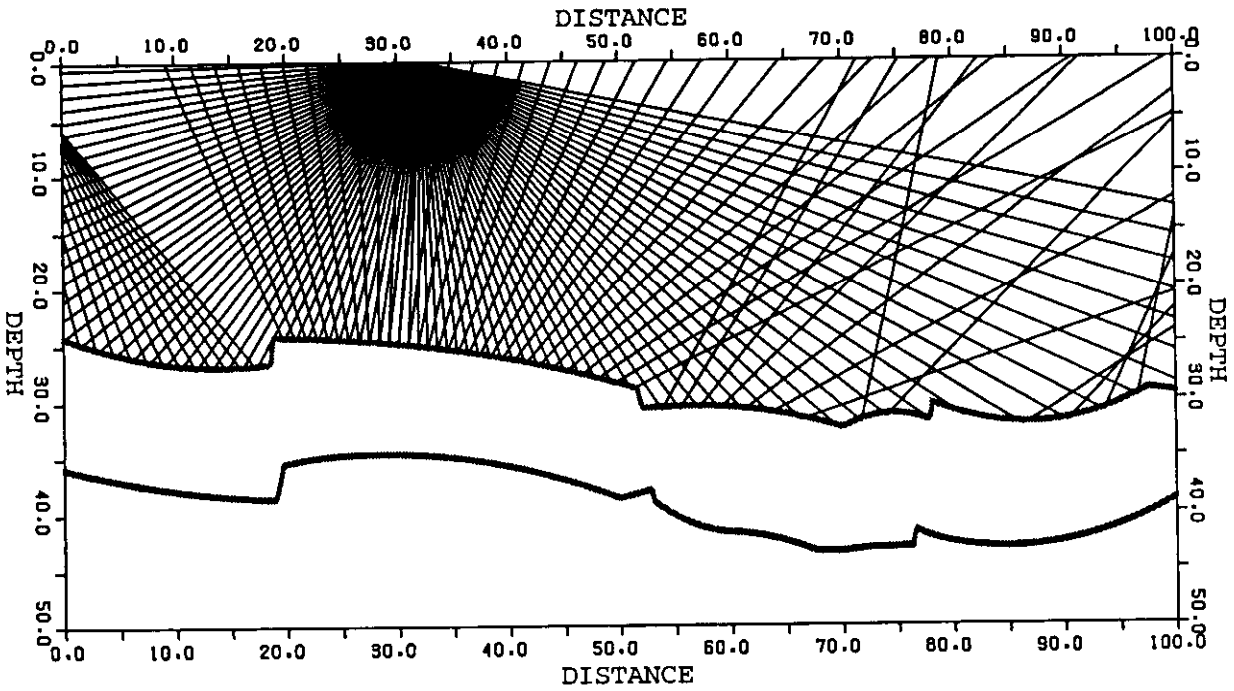

Fig. 6. Ray paths of the first unconverted P primaries computed for the third version of the simplified Southern Alberta crust, in which the interfaces were represented by the parabolic approximation computed for the tolerance parameter $\varepsilon = 0.4$. The geometrical shape of interfaces is the same as in Figure 5c, in which the input points specifying the boundaries are marked by crosses. The corresponding travel time curves and amplitude distance characteristics are shown in Figure 7a and 7b, respectively.

ferent numbers of simple travel time branches imply that a different number of events will also be seen on the corresponding computed synthetic traces. Perhaps, we can take comfort in seeing that all 5 simple travel time branches in Figure 7a can be located, although slightly shifted, in Figure 2b. Moreover, we find by comparing the pertinent amplitude distance curves in Figure 7b and Figure 3b, that the three strongest arrivals from Figure 7a also happen to be the strongest ones seen in Figure 2b. In other words, each of the three events corresponding to the three strongest unconverted primaries will be seen on the synthetic traces computed for both versions of the crustal model with the travel times and amplitudes being only slightly different. The minute differences in travel times and amplitudes in two models are caused by slightly different spatial locations of the intersections of the rays with two slightly different curves representing the same boundary in each of the two models. In particular, the slightly different lengths of the ray paths result in minute differences in travel times, whereas the slightly different curvatures of the interfaces at the respective points of incidence lead to different numerical values of the pertinent geometrical spreadings, which, in turn, yield slightly different amplitudes.

Table 2. Statistics for three different interface representations displayed in Figure 5. In the table, M represents the number of input points specifying the interface; N_{cs} is the number of cubic segments representing the interface in Figure 5a; $I_{0.1}$ and $I_{0.4}$ give the number of parabolic segments in the interface computed for two different values of $\varepsilon = 0.1$ and $\varepsilon = 0.4$ displayed in Figure 5b and 5c, respectively.

INTERFACE	M	N_{cs}	$I_{0.1}$	$I_{0.4}$
1	2	1	1	1
2	42	41	44	21
3	41	40	32	22

A more detailed investigation revealed that most of the 13 travel time branches seen in Figure 2b but having no counterparts in Figure 7a correspond to the ray paths reflected from highly curved sections of the interface which acted as efficient scatterers thereby producing small amplitudes of arrivals that would be hardly seen on the computed traces.

As the undulating character of the curve representing the interface is in fact controlled by the numerical value of ε (the smaller values of ε lead to higher local curvatures as two examples in Figure 5b and 5c indicate), it is recommended that initially larger values of ε (say $\varepsilon = 0.4$) be employed, followed by smaller values (say $\varepsilon = 0.1$) in the final stages of computation.

It is our experience that for the majority of typical models the numerical values of ε can be confined to the interval $0.1 \leq \varepsilon \leq 0.4$. These limits are also the two values used in Figure 5b and 5c for demonstration purposes.

Conclusions

In 2D models the seismic interfaces can be represented by continuous lines with at least the first order continuous derivatives if the diffracted waves are to be avoided. We have shown in this paper on numerical examples that the frequently used cubic spline representation of curved interfaces

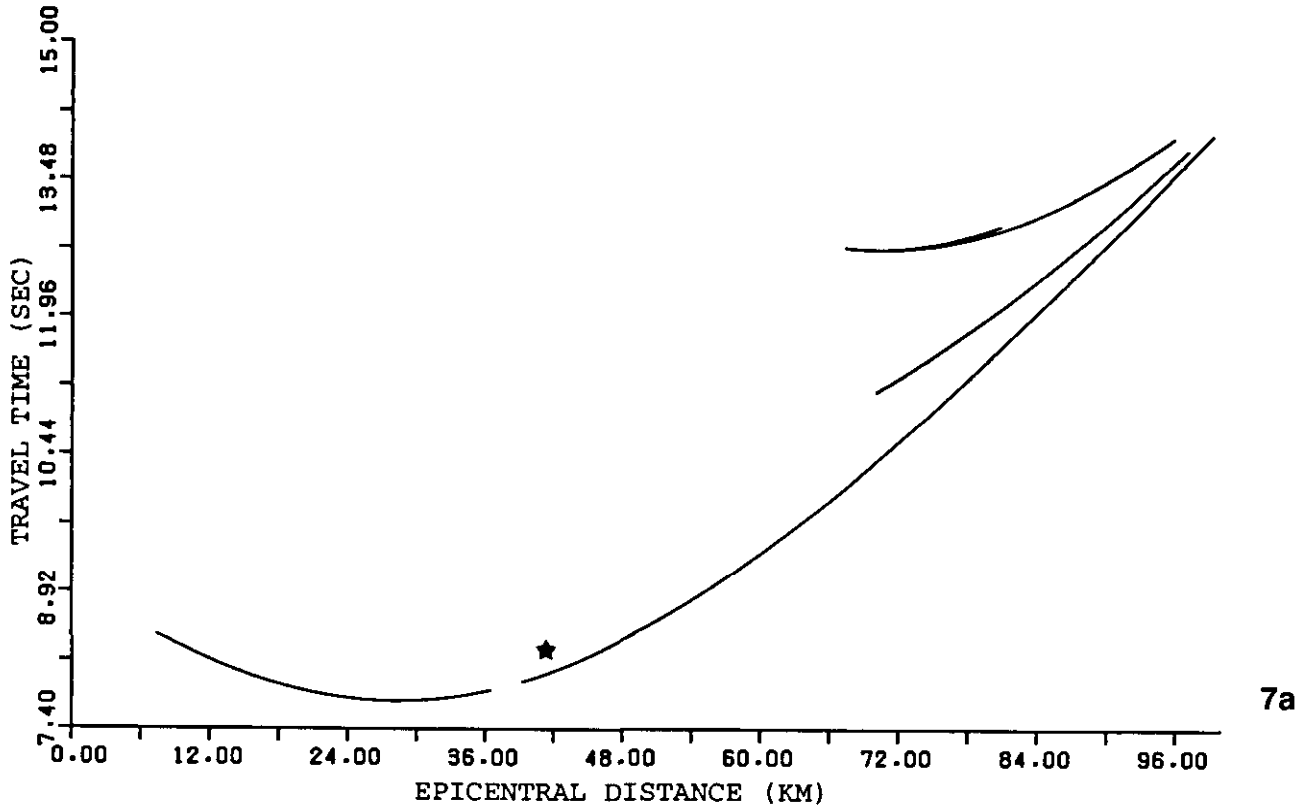

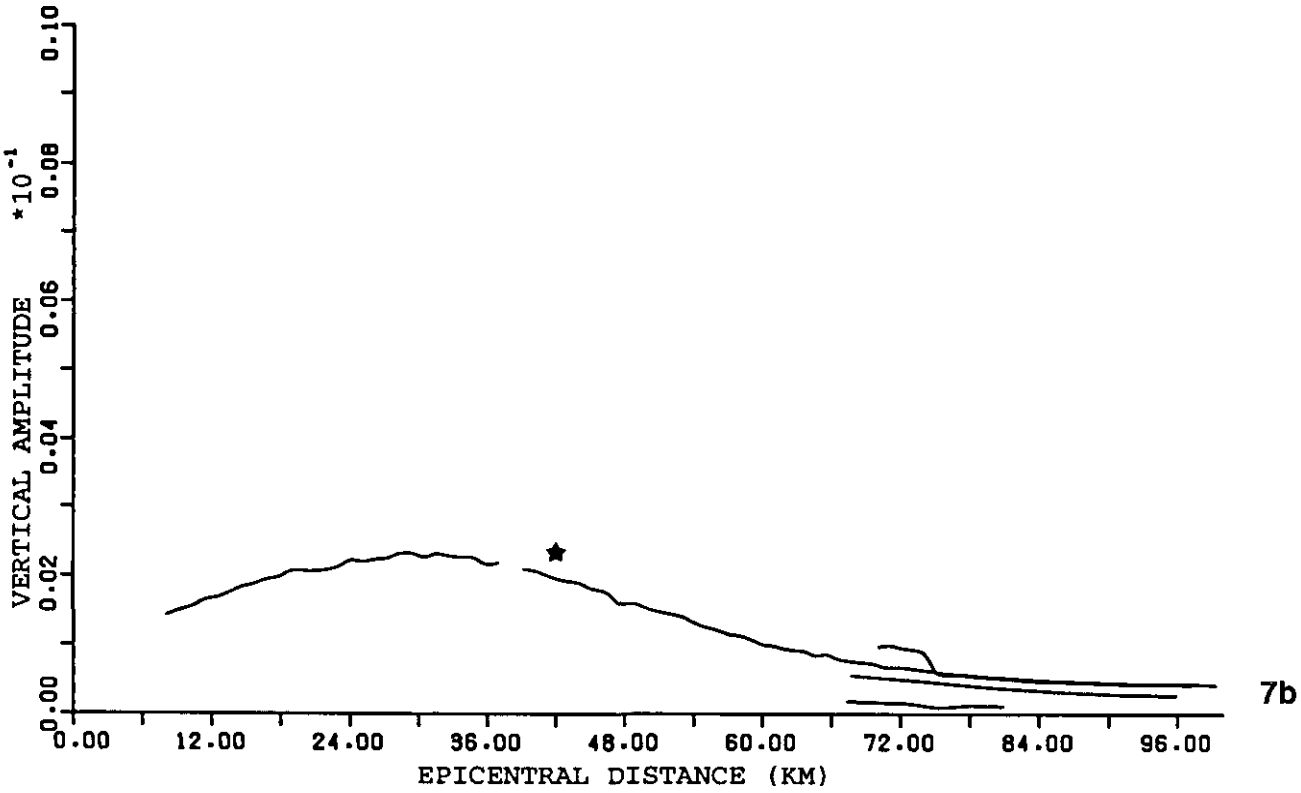

Fig. 7. Travel times and amplitudes of the first unconverted P primaries whose ray paths are shown in Figure 6. There are five separate travel times branches in Figure 7a with the corresponding amplitude distance curves in Figure 7b. The travel times and amplitudes of the first arrivals in the range from 38 km to 100 km are labelled by "*" to facilitate comparison with the similar curves in Figures 2 and 3.

is not convenient since it creates a conspicuous unrealistic overshooting if the interface is specified even by modestly scattered input points. This is due to two intrinsic properties of the cubic spline, namely to its continuity up to the second order derivatives and due to the fact that it passes through each input point of the set which it approximates. The resulting undulating shape of the approximated interface contributes to the occurrence of multiple arrivals of the same type of ray. This is seen on the examples of the first unconverted P primaries shown in the paper, and brings about major computational difficulties. These difficulties directly relate to the multiplicity of simple branches in the corresponding travel time curves which have to be rather precisely located before any two-point ray tracing procedure can be performed. Hence it is highly desirable to replace the cubic spline by an alternative technique which would eliminate overshooting caused by the cubic spline and provide some means by which the undulating shape of the approximated interface could be controlled.

In our opinion, based on long and extensive experience, such an alternative exists in the so-called parabolic approximation which was originally proposed in a relatively inaccessible Russian monograph by Marcinovskaya and Krasavin (1968) and whose basic mathematical properties are summarized for convenience in the Appendix. Formally, the parabolic approximation is based on second order polynomials which are not required to pass through every input point by being allowed to miss some of them within a prescribed tolerance governed by a special parameter ε closely related to the maximum permissible relative error (see Eq. A5). By increasing the numerical value of ε, the undulation of the approximating interface is suppressed and, as the presented numerical results testify, the multiplicity in travel time branches is reduced thereby decreasing even the number of multiple arrivals. The undesirable overshooting, which gave rise to spurious scattering of seismic energy, has been completely eliminated with the help of the so-called inserted parabolas which smoothly link any two adjacent sections of the interface with significantly different slopes. This process is discussed in the text and supported by the numerical examples presented in the paper.

References

Ahlberg, J.H., Nilson, E.N. and Walsh, J.L., 1967, The Theory of Splines and their Applications: Academic Press.

Babich, V.M. and Alekseev, A.S., 1958, A ray method of computing wave front intensities: Bull. Acad. Sci., U.S.S.R., Geophys. Ser. **1**, 9-15.

Cerveny, V. and Hron, F., 1980, The ray series method and dynamic ray tracing system for three-dimensional inhomogeneous media: Bull. Seism. Soc. Am., **70**, 47-77.

_____ and Ravindra, R., 1971, Theory of seismic head waves: University of Toronto Press.

Choi, A.P. and Hron, F., 1981, Amplitude and phase shift due to caustics: Bull. Seism. Soc. Am, **71**, 1445-1461.

Forsythe, G.E., Malcolm, M.A. and Moler, C.B., 1977, Computer methods for mathematical computations: Prentice-Hall.

Hron, F., 1968, Introduction to the ray theory in a broader sense: Application to Seismology: Textbook of Laboratorie de Physique de l'Ecole Normale Superiéure, Université de Paris.

_____, 1971, Criteria for selection of phases in synthetic seismograms for layered media: Bull. Seism. Soc. Am., **61**, 765-779.

_____, 1972, Numerical methods of ray generation in multilayered media, *in*: Methods in Computational Physics 12 (Alder, B., Fernbach, S. and Bolt, B.A., Eds.): Academic Press Inc., 1-34.

_____, 1973, A numerical ray generation and its application to the computation of synthetic seismograms for complex layered media: Geophys. J.R. astr. Soc., **35**, 345-349.

_____, Daley, P.F. and Marks, L.W., 1977, Numerical modeling of seismic body waves in oil exploration and crustal seismology, *in*: Proceedings of American Soc. of Mechanical Engineers Symposium on Computing Methods in Geophysical Mechanics: AMD, **25**, 21-42.

_____ and Kanasewich, E.R., 1971, Synthetic seismograms for deep seismic sounding studies using Asymptotic Ray Theory: Bull. Seism. Soc. Am., **61**, 1169-1200.

_____, _____ and Alpaslan, T., 1974, Partial ray expansion required to suitably approximate the exact wave solution: Geophys. J.R. astr. Soc., **36**, 607-625.

_____, May, B.T., Covey, J.D. and Daley, P.F., 1986, Synthetic seismic sections for acoustic, elastic, anisotropic and vertically inhomogeneous layered media: Geophysics, **51**, 710-735.

Kanasewich, E.R., 1968, Precambrian rift: Genesis of strata-bound ore deposits: Science, **161**, 1002-1005.

Marcinovskaya, N.G. and Krasavin, V.G., 1968, Algorithm for computing the reflected wave field in media with curved boundaries, *in*: Problems in the Dynamic Theory of Seismic Wave Propagation (Petrashen, G.I., Ed.) 9: Nauka, Leningrad, 135-144.

Zhou, H.S., 1996, Numerical modeling of seismic waves in 2D inhomogeneous structures using Asymptotic Ray Theory: M.Sc. thesis, University of Alberta.

Appendix

Approximation of two-dimensional sets of discrete points by second order polynomials with continuous derivatives

A method of piecewise approximation of curvilinear boundaries by a group of parabolas linked smoothly together was suggested by Marcinovskaya and Krasavin (1968). Since this paper is for the majority of English speaking readers relatively inaccessible, a brief description of the method together with some basic formulae is presented next.

Suppose the set of M discrete points specified by their Cartesian coordinates in a two-dimensional coorinate system $[\xi_m, \zeta_m]$, m = 1, ..., M.

The simplest approximation of these points by a continuous curve f(x) can be achieved over the interval $< X_{min}, X_{max} >$, where $X_{min} = \text{Min}\ (\xi_m)$, $X_{max} = \text{Max}\ (\xi_m)$, m = 1, ..., M, with the help of I parabolas

$$z_i(x) = a_i x^2 + b_i x + c_i, \quad i = 1, ..., I, \tag{A1}$$

each of them being defined over the interval

$$< X_i, X_{i+1} > \tag{A2}$$

provided that

$$z_i (X_{i+1}) = z_{i+1} (X_{i+1}),$$

$$\left.\frac{dz_i}{dx}\right|_{x = X_{i+1}} = \left.\frac{dz_{i+1}}{dx}\right|_{x = X_{i+1}}. \tag{A3}$$

The three coefficients a_i, b_i and c_i determining the parabola (A1) over its region of definition (A2) have to be determined

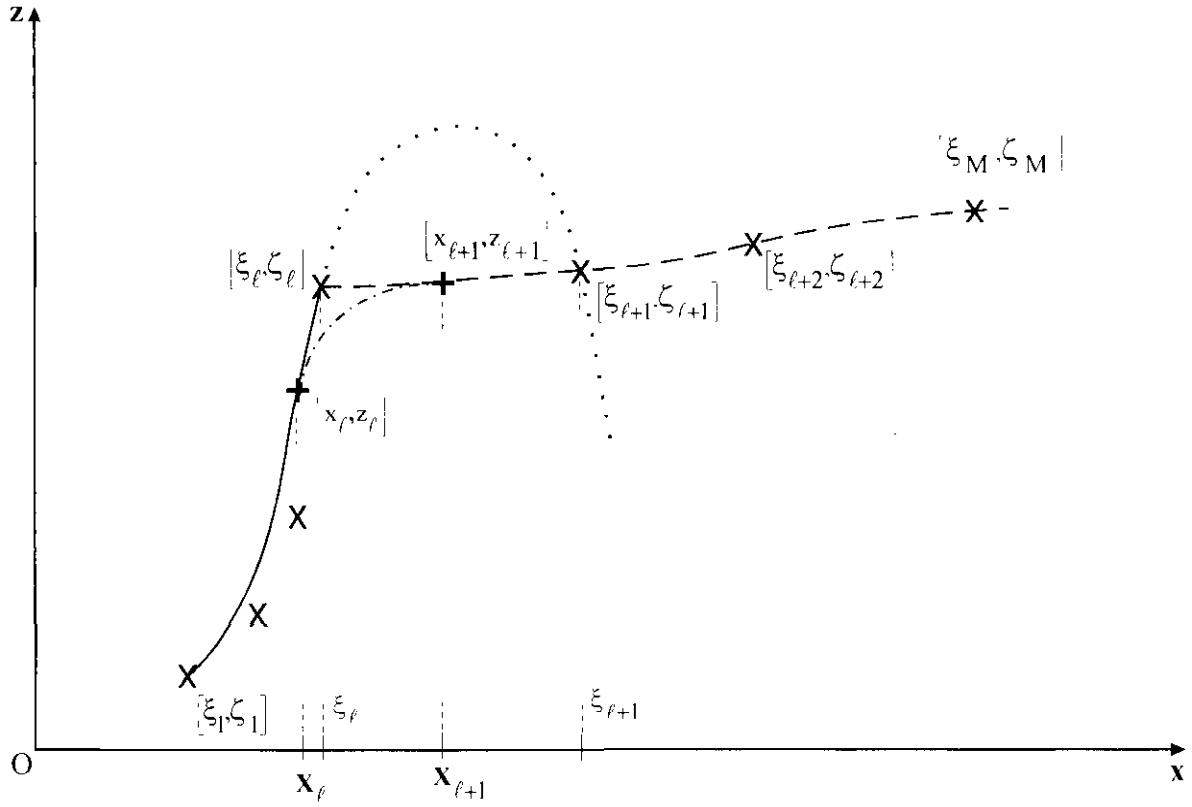

Fig. A1. A spurious local extreme (referred to as "overshooting" in the text) between two input points $[\xi_\ell,\zeta_\ell]$ and $[\xi_{\ell+1},\zeta_{\ell+1}]$ is removed with the help of an inserted parabola defined over the interval $[X_\ell, X_{\ell+1}]$. It smoothly links adjacent parabolas with significantly different slopes.

from a system of 3 linearly independent equations. For the first parabola such a system is easily obtained by simultaneously applying (A1) to the first 3 points of the set $[\xi_m, \zeta_m]$, m = 1, 2, 3, and by accepting $X_1 = \xi_1$ and $X_2 = \xi_3$ as the lower and upper bound of the interval (A2).

It is obvious that the continuity of the curve will be preserved if during a repetitive cycle the coefficients of the (i+1) -th parabola are computed with the help of the previous parabola already obtained by solving the system

$$\begin{aligned} &a_{i+1}\, X_{i+1}^2 + b_{i+1}\, X_{i+1} + c_{i+1} = z_i\,(X_{i+1})\,, \\ &a_{i+1}\, \xi_m^2 + b_{i+1}\, \xi_m + c_{i+1} = \zeta_m\,, \\ &2a_{i+1}\, X_{i+1} + b_{i+1} = \left.\frac{dz_i}{dx}\right|_{x\,=\,X_{i+1}}\,, \end{aligned} \qquad \text{(A4)}$$

where $[\xi_m, \zeta_m]$, are the coordinates of the next input point for which we also set $X_{i+2} = \xi_m > X_{i+1}$.

If the system (A4) were solved for all (M-1) pairs of adjacent points, two rather unpleasant features of such an approach would be discovered:

(1) the method would not be very practical, especially for large numbers of input points;

(2) in the case of widely scattered input points $[\xi_m, \zeta_m]$ the curve will become a rather inconvenient representation of the seismic boundary due to its necessarily widely undulating shape characterized by pronounced local maxima and minima (see Fig. A1) that would make the two point ray tracing procedure quite difficult.

The first problem can be solved easily if one is satisfied with the curve missing some input points within a specified tolerance while preserving the main geometric shape represented by the points.

In such case the system (A4) is solved by using coordinates $[\xi_m, \zeta_m]$ of a more distant input point (say the last one). If the relative error between the computed z and the input ζ coordinates is smaller than a certain input value ε for all points from the open interval (X_{i+1}, ξ_m), i.e., if

$$\left| \frac{a_{i+1}\, \xi_j^2 + b_{i+1}\, \xi_j + c_{i+1} - \zeta_j}{\mathrm{Max}(\zeta_j) - \mathrm{Min}(\zeta_j)} \right| \le \varepsilon\,,\ X_{i+1} < \xi_j < \xi_m = X_{i+2}\,, \qquad \text{(A5)}$$

then the values a_{i+1}, b_{i+1}, c_{i+1} and ξ_m are accepted as the coefficients of the (i+1) -th parabola, and the right bound X_{i+2} of its definition interval $< X_{i+1}, X_{i+2} >$, respectively. In this way the total number of approximating parabolas is significantly reduced.

The second problem, the problem of undulating shape of the approximating curve, which is the result of its distinct local minima and maxima, can be solved by the insertion of a few additional parabolas that will eliminate these extrema. It is clear that the method designed for the reduction of the

total number of parabolas fails when z-coordinates of the input points are scattered over a large interval as in Figure A1. It shows the case which would result in a spurious maximum on the ℓ-th parabola, if a standard procedure based on the system (A4) is applied to two points with coordinates $[\xi_\ell,\zeta_\ell]$ and $[\xi_{\ell+1},\zeta_{\ell+1}]$.

Such unjustified and therefore undesirable local extreme, which is clearly an artifact of the parabolic spline approximation, can be avoided by the following two step procedure, the results of which are schematically depicted in Figure A1:

First we will find a parabola passing through three consecutive points $[\xi_\ell,\zeta_\ell],[\xi_{\ell+1},\zeta_{\ell+1}]$ and $[\xi_{\ell+2},\zeta_{\ell+2}]$ by solving the system

$$\begin{aligned} a_{\ell+1}\xi_\ell^2 + b_{\ell+1}\xi_\ell + c_{\ell+1} &= \zeta_\ell \\ a_{\ell+1}\xi_{\ell+1}^2 + b_{\ell+1}\xi_{\ell+1} + c_{\ell+1} &= \zeta_{\ell+1} \\ a_{\ell+1}\xi_{\ell+2}^2 + b_{\ell+1}\xi_{\ell+2} + c_{\ell+1} &= \zeta_{\ell+2}. \end{aligned} \tag{A6}$$

Then the two already determined parabolas with coefficients $a_{\ell-1},b_{\ell-1},c_{\ell-1}$ and $a_{\ell+1},b_{\ell+1},c_{\ell+1}$ will be linked smoothly together by an inserted parabola, whose coefficients are

$$\begin{aligned} a_\ell &= \frac{-2a_{\ell-1}X_\ell + 2a_{\ell+1}X_{\ell+1} - b_{\ell-1} + b_{\ell+1}}{2(X_{\ell+1} - X_\ell)} \\ b_\ell &= 2(a_{\ell+1} - a_\ell)X_{\ell+1} + b_{\ell+1} \\ c_\ell &= (a_\ell - a_{\ell+1})X_{\ell+1}^2 + c_{\ell+1}, \end{aligned} \tag{A7}$$

and which is defined over the range

$$< X_\ell, X_{\ell+1} >. \tag{A8}$$

The right bound of the inserted interval is given by

$$X_{\ell+1} = \frac{2(c_{\ell+1} - c_{\ell-1}) + (b_{\ell+1} - b_{\ell-1})X_\ell}{2(a_{\ell-1} - a_{\ell+1})X_\ell + b_{\ell-1} - b_{\ell+1}} \tag{A9}$$

while its left bound is defined as

$$X_\ell = \xi_\ell - \Delta x. \tag{A10}$$

The quantities a_ℓ,b_ℓ,c_ℓ from (A7), which are together with $X_{\ell+1}$ the solutions of the following system of four algebraic equations (with $\mathbf{X}_\ell$ as a parameter),

$$\begin{aligned} a_{\ell-1}X_\ell^2 + b_{\ell-1}X_\ell + c_{\ell-1} &= a_\ell X_\ell^2 + b_\ell X_\ell + c_\ell \\ 2a_{\ell-1}X_\ell + b_{\ell-1} &= 2a_\ell X_\ell + b_\ell \\ a_\ell X_{\ell+1}^2 + b_\ell X_{\ell+1} + c_\ell &= a_{\ell+1}X_{\ell+1}^2 + b_{\ell+1}X + c_{\ell+1} \\ 2a_\ell X_{\ell+1} + b_\ell &= 2a_{\ell+1}X_{\ell+1} + b_{\ell+1}, \end{aligned} \tag{A11}$$

are accepted as the coefficients of the ℓ-th parabola only if the bounds of the inserted interval (A9) and (A10) satisfy the relation

$$X_\ell < \xi_\ell < X_{\ell+1} < \xi_{\ell+1}, \tag{A12}$$

which is achieved by a suitably selected value of Δx in (A10).